Dominant Influence of ENSO-Like and Global Sea Surface Temperature Patterns on Changes in Prevailing Boreal Summer Tropical Cyclone Tracks over the Western North Pacific

Haikun Zhao

Key Laboratory of Meteorological Disaster, Ministry of Education, and Joint International Research Laboratory of Climate and Environment Change, and Collaborative Innovation Center on Forecast and Evaluation of Meteorological Disaster, and Pacific Typhoon Research Center, Nanjing University of Information Science and Technology, Nanjing, and State Key Laboratory of Tropical Oceanography, South China Sea Institute of Oceanology, Chinese Academy of Sciences Guangzhou, China

Philp J. Klotzbach

Department of Atmospheric Science, Colorado State University, Fort Collins, Colorado

Shaohua Chen

Key Laboratory of Meteorological Disaster, Ministry of Education, Pacific Typhoon Research Center, Nanjing University of Information Science and Technology, Nanjing, China

ABSTRACT: A conventional empirical orthogonal function (EOF) analysis is performed on summertime (May–October) western North Pacific (WNP) tropical cyclone (TC) track density anomalies during 1970–2012. The first leading EOF mode is characterized by a consistent spatial distribution across the WNP basin, which is closely related to an El Niño–Southern Oscillation (ENSO)-like pattern that prevails on both interannual and interdecadal time scales. The second EOF mode is represented by a tripole pattern with consistent changes in westward and recurving tracks but with an opposite change for west-northwestward TC tracks. This second EOF pattern is dominated by consistent global sea surface temperature anomaly (SSTA) patterns on interannual and interdecadal time scales, along with a long-term increasing global temperature trend. Observed WNP TC tracks have three distinct interdecadal epochs (1970–86, 1987–97, and 1998–2012) based on EOF analyses. The interdecadal change is largely determined by the changing impact of ENSO-like and consistent global SSTA patterns. When global SSTAs are cool (warm) during 1970–86 (1998–2012), these SSTAs exert a dominant impact and generate a tripole track pattern that is similar to the positive (negative) second EOF mode. In contrast, a predominately El Niño–like SSTA pattern during 1987–97 contributed to increasing TC occurrences across most of the WNP during this 11-yr period. These findings are consistent with long-term trends in TC tracks, with a tripole track pattern observed as global SSTs increase. This study reveals the potential large-scale physical mechanisms driving the changes of WNP TC tracks in association with climate change.

KEYWORDS: ENSO; Tropical cyclones; Climate variability

1. Introduction

The accurate prediction and forecasting of tropical cyclone (TC) tracks are fundamental and are important for the prevention and mitigation of TC-associated disasters. The western North Pacific (WNP) is the most active basin on an annually averaged basis, with ~25.5 TCs ($\geq 17\,\mathrm{m\,s^{-1}}$) occurring per year based on data from the Joint Warning Typhoon Center (JTWC) best track dataset (Chu et al. 2002; https://www.metoc.navy.mil/jtwc/jtwc.html) using a 1970–2012 climatology. These results are similar to what was found by Schreck et al. (2014) using a 1981–2010 climatology. Tropical cyclones can cause tremendous economic damage and pose a great threat to human life in China and adjacent countries (Zhang et al. 2009, 2011). It has been well documented that there is considerable variability in WNP TC tracks ranging from intraseasonal (Camargo et al. 2007a; Chen et al. 2009; Li and Zhou 2013), to interannual (Wang and Chan 2002; Zhao et al. 2010, 2011) to interdecadal and decadal time scales (Wu and Wang 2004; Ho et al. 2004; Fudeyasu et al. 2006; Chan 2008; Liu and Chan 2008; Zhao et al. 2014). Changing atmospheric and oceanic conditions on these time scales can cause changes in TC track, TC intensity, and the regions most likely to be influenced by TCs (Zhao et al. 2010, 2011, 2014; Wang et al. 2011; Wu and Zhao 2012; Zhao and Wu 2014; Zhao 2016; Wu et al. 2018). An in-depth understanding of how changes in the large-scale climate impact WNP TC tracks therefore is of importance both socioeconomically as well as scientifically.

El Niño–Southern Oscillation (ENSO) has been demonstrated in many prior studies to be an important interannual factor affecting WNP TC formation location, track, and intensity (Lander 1994; Wang and Chan 2002; Elsner and Liu 2003; Camargo and Sobel 2005; Kim et al. 2010; Zhao et al.

2010, 2011, 2014; Zhan et al. 2011; Ha et al. 2013; Zhao and Wu 2014; Zhao and Wang 2016, 2019; Hu et al. 2018; Wang et al. 2019; Wang and Wang 2019). These papers have documented that there is a southeastward shift in TC formation location and that the TCs that form tend to last longer and become stronger during El Niño years than during La Niña years (Wang and Chan 2002; Camargo and Sobel 2005; Zhao et al. 2011; Zhao and Wang 2016). Meanwhile, more TCs during El Niño years tend to recurve northward and thus significantly impact East Asian coastal areas (Saunders et al. 2000; Wang and Chan 2002; Wu and Wang 2004; Fudeyasu et al. 2006; Camargo et al. 2007b).

Several studies have suggested that WNP TC tracks have obvious interdecadal variability. These studies found that this interdecadal variability was closely related to changes in the strength and intensity of the WNP subtropical high and monsoon circulation changes driven by the Pacific decadal oscillation (PDO) and the interdecadal Pacific oscillation (IPO) (Ho et al. 2004; Wu et al. 2005; Chan 2008; Liu and Chan 2008; Tu et al. 2009; Zhao and Wu 2014; Hu et al. 2018). For example, from the late 1990s to the mid-2010s, TC genesis frequency over the WNP basin showed a significant reduction, and TC formation locations shifted westward with more TCs affecting East Asia and Taiwan. This shift was attributed to a strengthening of the WNP subtropical high, a weakening Asian summer monsoon trough, and a reduced positive vorticity anomaly in the lower troposphere. Changes in the large-scale environment were largely attributed to the phase change of the PDO and IPO from warm to cool (Chan 2008; Liu and Chan 2008; Zhao and Wang 2016, 2019; Zhao et al. 2018; Hu et al. 2018). Significant impacts of the phase change in the PDO and IPO on TC tracks were also found over the eastern North Pacific and the North Atlantic (Li et al. 2015).

Over the past several decades, much attention has been paid to the impact of climate change on weather and climate events (IPCC 2013; Knutson et al. 2019, 2020). Many studies have attempted to understand the possible impact of global warming on TC activity over the WNP basin as well as other TC basins (Wang et al. 2011; Wu et al. 2015; Camargo et al. 2016; Zhao et al. 2009; Knutson et al. 2010; Murakami et al. 2011, 2018). Several studies have indicated that climate change may have already had a detectable impact on TC activity, especially with regard to TC intensity (Knutson and Tuleya 2004; Emanuel 2005; Webster et al. 2005; Wu and Wang 2008; Wu et al. 2008, 2018; Knutson et al. 2020). Changes in TC tracks in response to global warming have been relatively less studied. Wu and Wang (2004) assessed the possible impact of global warming on the prevailing tracks of WNP TCs by using the large-scale environment derived from the NOAA Geophysical Fluid Dynamics Laboratory global warming experiment. Based upon analyses of both observations as well as several climate models from the IPCC, Wang et al. (2011) suggested that global warming appeared to play an important role in changing WNP TC tracks.

Most of these previous studies have focused on the possible impact of various climate modes at different time scales (e.g., interannual, interdecadal, and climate change) on WNP TC tracks, while few studies have investigated the prevailing modes of WNP TC tracks and the relative importance of

associated climate variability in driving changes in WNP TC tracks. The main objectives of this study are twofold. First, we explore various climate modes and their influence on summertime TC track changes over the WNP basin. We also evaluate potential associated physical mechanisms. Second, we examine the relative importance of these identified modes in modulating observed changes in summertime WNP TC tracks as well as their long-term trends. We also provide plausible physical explanations for our results.

The remainder of this study is organized as follows. Section 2 describes the data and methodology. Section 3 identifies the major modes of WNP summertime TC tracks and further investigates the likely drivers of these TC track modes. Section 4 assesses the respective importance of the identified TC track modes in contributing to interdecadal changes in summertime WNP TC tracks as well as the long-term trend of WNP TC tracks. Section 5 summarizes our findings.

2. Data and methodology

a. Atmospheric and oceanic data

Atmospheric fields are derived from the National Centers for Environmental Prediction–Department of Energy monthly reanalysis (NCEP–DOE) with 2.5° latitude × 2.5° longitude horizontal resolution and 17 vertical levels (Kanamitsu et al. 2002). Monthly sea surface temperatures (SSTs) are calculated from the NOAA Extended Reconstructed SST version 4 (ERSST v4) dataset (Huang et al. 2015; Liu et al. 2015). The Niño-3.4 SST index, defined to be SSTs in the region bounded by 5°S–5°N, 170°–120°W, was downloaded from NOAA's Climate Prediction Center (https://www.esrl.noaa.gov/psd/data/correlation/nina34.data). This index has been adopted in previous studies to define the ENSO state (Wang and Chan 2002; Camargo and Sobel 2005). The PDO index is obtained from the Joint Institute for the Study of the Atmosphere and Ocean of the University of Washington (http://research.jisao.washington.edu/pdo/). The PDO index is defined as the leading principal component (PC) of North Pacific (poleward of 20°N) monthly SST anomaly (SSTA) variability (Mantua et al. 1997).

b. TC data

TC data are obtained from the JTWC best track dataset website https://www.metoc.navy.mil/jtwc/jtwc.html (Chu et al. 2002). This dataset provides TC information including latitude, longitude, and maximum sustained wind speed (MSW) at a 6-h interval. All TCs reaching at least tropical storm intensity (i.e., MSW $\geq$ 17 m s^{-1}) from May to October are considered in this study. We define May–October as the summer for two main reasons. One reason is that there is an annual average of 20.3 TCs during May–October, accounting for ~80% of the annually averaged total number of TCs during 1970–2012. Additionally, TC activity is so frequent in the summertime that the climatological mean winds can well represent the large-scale steering flow (Wu and Wang 2004). Two other best track datasets—the Shanghai Typhoon Institute/China Meteorological Administration (STI_CMA) and the Japan Meteorological Agency (JMA) (Zhan et al. 2011; Schreck et al. 2014)—were also used to investigate the influence of climate change on TC activity. We also conducted additional
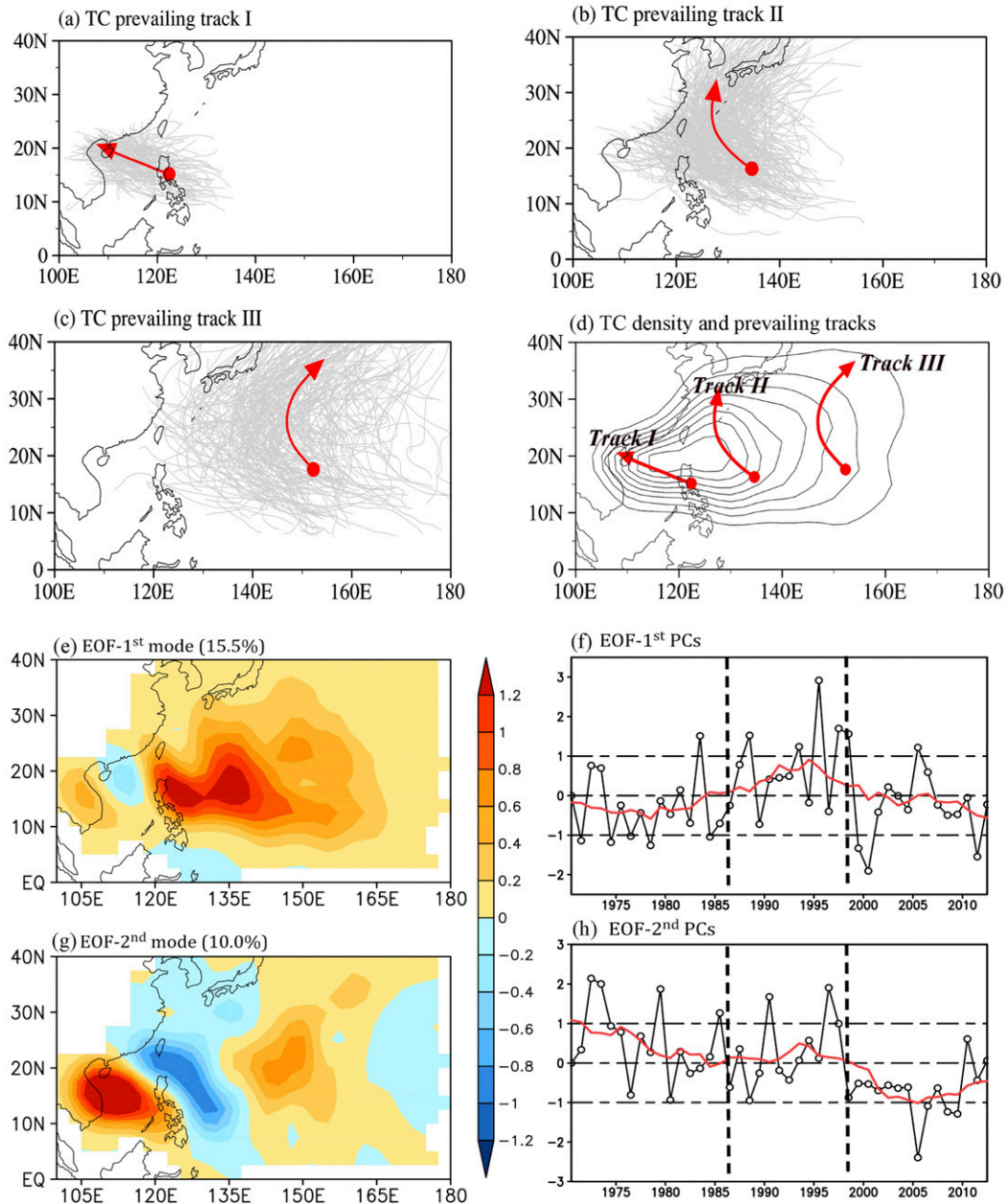
FIG. 1. (a)–(c) Western North Pacific TC tracks for the three *k*-means clusters (in gray) during the period from 1970 to 2012. The prevailing TC tracks in red for each cluster are the centers of each cluster. (d) Climatological summertime (May–October) TC track density over the WNP basin during 1970–2012 along with the three prevailing TC tracks in red arrows. (e) First and (g) second leading EOF modes of summertime (May–October) TC track density over the western North Pacific during 1970–2012 with their corresponding explained variance (%) in parentheses. Time series of principal components of the (f) first and (h) second EOF modes of summertime (May–October) typhoon tracks over the western North Pacific during 1970–2012 displayed in black lines with open dots. The corresponding 9-yr moving averages of these principal components are plotted with red lines.

analysis using these two datasets and found broad consistency among the three best track datasets. The consistency of the results confirms that the results on TC track changes are not sensitive to which TC dataset is used. Unless stated otherwise, we show results using the JTWC best track dataset for the remainder of this manuscript.

c. EOF analysis of TC tracks

The conventional empirical orthogonal function (EOF) method has been widely used in atmospheric and oceanic analyses as a compact description of the spatiotemporal variability of separated statistical modes (Rasmusson et al. 1981; Anderson and Gyakum 1989; Lee and Cornillon 1995;

Liu and Chan 2008; Wang et al. 2008; Kim et al. 2010). In this study, an EOF analysis of summertime TC track density anomalies during 1970–2012 over the WNP basin is performed to identify the principal components (PCs) of TC track pattern changes.

Since there are several grid points each year in the WNP basin with no TC tracks that may cause the leading modes to render physically meaningless patterns, the overlap-gridding technique following Kim et al. (2010) is used to smooth sporadic TC occurrence points and thus solve the problem arising from the discrete gridding technique. In this study, we successively shifted each grid box at a 2.5° interval in latitude and longitude.

We focus on the period from 1970–2012 in this study for two main reasons. When using EOF analyses of boreal summer TC track density anomalies, there are four distinct interdecadal regimes (1970–86, 1987–97, 1998–2012, and 2013–18) that occur. However, the last of these (2013–18) is much shorter than a decade. In addition, when extending our results to 2018 and including both the STI_CMA and JMA best track datasets, we obtain almost identical results for the two EOFs that we identify in the following sections when focusing on 1970–2012.

d. Statistical significance test

The two-tailed Student's t test is used to examine statistical significance for the correlation and composite analyses. In this study, p values equal to or less than 0.05 are deemed statistically significant. The threshold correlation coefficient for significance is 0.30 for the whole period of 1970–2012 (43 years). A 9-yr running average is used to calculate interdecadal correlations.

3. Two prevailing modes of WNP summertime TC tracks and the associated possible large-scale driving mechanisms

In this study, all variables are averaged from May to October. Following previous studies (Elsner and Liu 2003; Elsner 2003), a k-means clustering method has been adopted to identify the three prevailing TC tracks over the WNP basin. Equal data lengths for all of the target objects are needed when using the k-means clustering algorithm. In this study, we artificially interpolate every TC track into 19 segments (20 data points) with equal length by leaving out time information following Kim et al. (2011) and Kim and Seo (2016). As shown in Fig. 1a, a westward prevailing track extends from the tropical WNP to the Philippine Sea and the South China Sea (SCS) (hereafter track I). The northwestward prevailing track extends from the tropical WNP to the Korean peninsula and Japan (hereafter track II) (Fig. 1b), and the third prevailing track tends to recurve northeastward east of 145°E (hereafter track III) (Fig. 1c). The three defined prevailing TC tracks are matched with the ridge of TC track density (Fig. 1d), implying a reasonable representation of the three identified TC prevailing tracks. The track density is counted at a 6-h interval for each 2.5° latitude × 2.5° longitude grid box during 1970–2012. The frequency of TC occurrence indicates how often TCs affect a specific grid box. A similar representation of climatological prevailing TC tracks over the WNP basin has also been

adopted in previous studies (Wu and Wang 2004; Wu et al. 2005; Liu and Chan 2008; Wang et al. 2011). Considering the possible impact of seasonal changes in TC tracks, the prevailing TC tracks over the WNP basin during different seasons (May–July and August–October) have been further examined, and no substantial difference are observed (Fig. S1 in the online supplemental material). The three prevailing TC tracks during these two 3-month periods are very similar. The latitude of the recurving point during August–October tends to be more northward than during May–July, which may be associated with differences in the large-scale flow.

As shown in Figs. 1e and 1g, changes in TC tracks over the WNP basin during 1970–2012 can be represented by two distinct EOF patterns with explained variances of 15.5% and 10.0%, respectively. The first EOF (EOF-1st mode) is relatively well separated from the second (EOF-2nd) mode as shown in Figs. 1e and 1g, although they fail to attain a complete separation beyond a 95% confidence error limit using the rule of the thumb (North et al. 1982). To test whether the leading EOF patterns are robust, regardless of the length of the period of interest, we have performed EOF analyses multiple times using subsets of the years from 1970 to 2018. Similar patterns for the first two leading EOF modes are obtained regardless of the data sample used. Figure 2 shows the first two EOF modes of track density anomalies over the WNP basin during 1970–86, 1970–97, 1970–2012, and 1970–2018, respectively. A similar consistent basinwide pattern for the EOF-1st mode appears during each of these subperiods, implying that a basinwide consistent EOF mode is not sensitive to the selected period (Figs. 2a,c,e,g). Figure 2 also displays the EOF-2nd mode, which exhibits a tripole pattern during each of these subperiods, although there are some differences observed during 1970–86. As suggested by Liu and Chan (2008) and Mei et al. (2015), the results based on EOF analyses may be somewhat sensitive to the study period being investigated. Similarly, this study found that these two EOF modes are dominant during the period of 1970–86 and 1998–2012, while the EOF-1st mode appears to be more important during the period of 1987–97 (Fig. 1). These results compare well with the results of EOF analyses of TC tracks for different periods (Fig. S2). Of course, changes in TC tracks over the WNP basin during May–October are determined by more than just changes in TC tracks associated with the two leading EOF-modes shown in Fig. 2. Note that this study focuses on the EOF-1st and EOF-2nd modes of TC tracks during 1970–2012 and systematically attempts to understand the relative importance of these two EOF modes in TC tracks during these different decades. While there are some differences between the two different seasons, these impacts generally appear limited to the first two EOF modes calculated in our analyses. In this sense, no significant statistical separation of eigenvalue between the first two EOF modes following the rule of thumb proposed by North et al. (1982) does not mean that the modes are unphysical, but rather that these two EOF modes may be a possible distortion of the real pattern.

Also shown in Fig. 1e, the EOF-1st mode is a consistent spatial pattern across most of the WNP basin except for a change to the opposite sign over the northern SCS. The
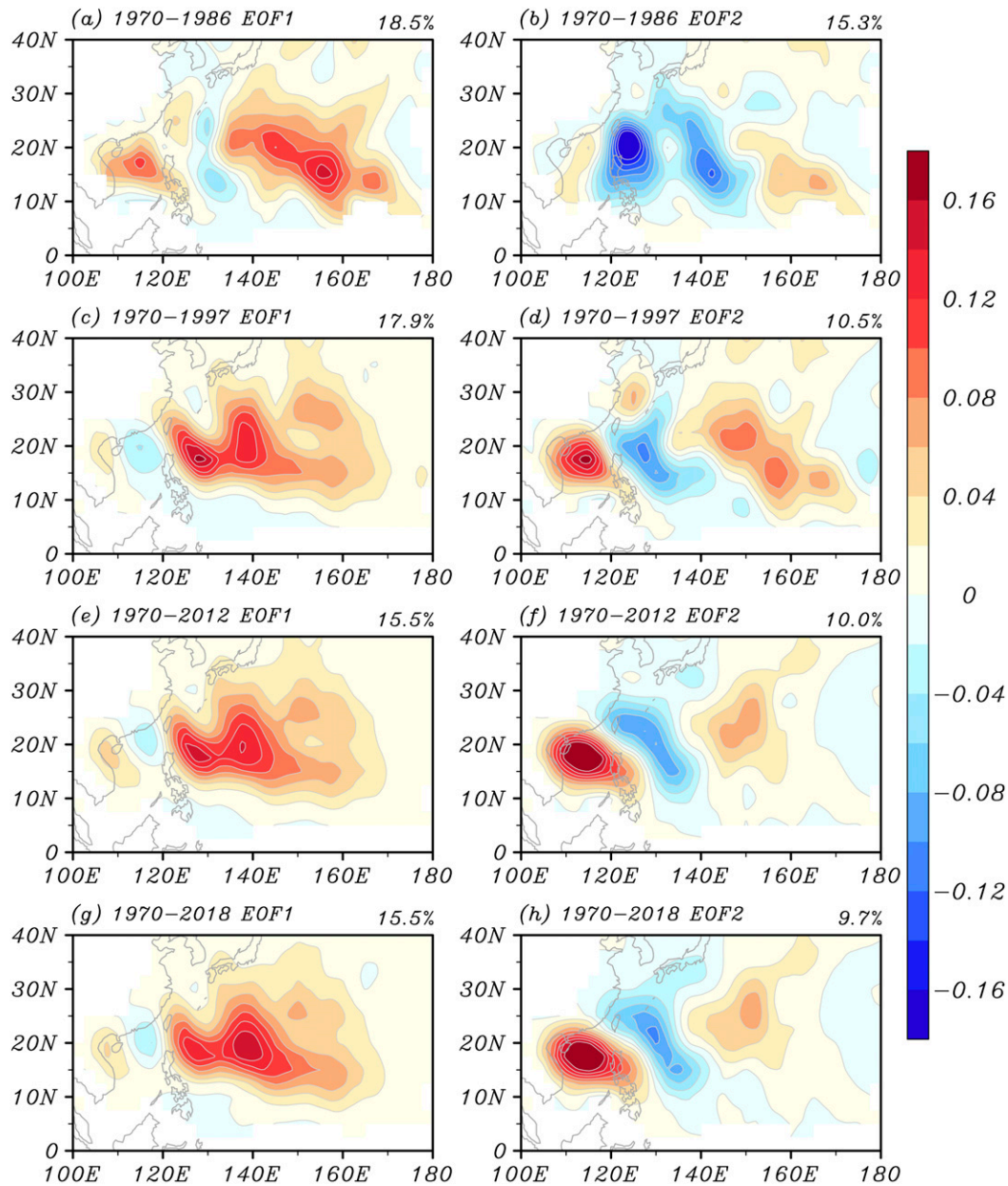
FIG. 2. The first two leading EOF modes of extended boreal summer (May–October) TC track density anomalies during (a),(b) 1970–86, (c),(d) 1970–97, (e),(f) 1970–2012, and (g),(i) 1970–2018. The corresponding explained variances of each EOF mode are listed at the top-right corner of each panel.

EOF-1st mode indicates more (fewer) TCs taking prevailing northwestward or recurving tracks (tracks II and III) and slightly fewer (more) TC occurrences in the northern SCS (track I). In contrast, the EOF-2nd mode is a tripole pattern in TC tracks, with consistent changes (i.e., consistent increases/decreases in TC occurrences) over the region from the Philippines to the SCS and the eastern (east of ~145°E) part of the WNP basin with an opposite change for TC occurrences (i.e., consistent decrease/increase in TC occurrences) from the tropical WNP (from ~125° to 140°E) to the Korean peninsula

and Japan (Fig. 1g). There is a systematic change in the climatological prevailing TC tracks, with an increase or a decrease of the prevailing westward track (track I) and recurving track (track III) and a respective decrease or increase of the prevailing northwestward track (track II).

We also further compare with previous studies that applied EOF analysis to explore variations in WNP TC tracks (Liu and Chan 2008; Mei et al. 2015). A consistent basinwide pattern for the first EOF mode is similar to the spatial pattern of the first EOF mode for high-pass-filtered and low-pass-filtered track

(a) Pacific mode: PC1 vs. SST (Correlation)

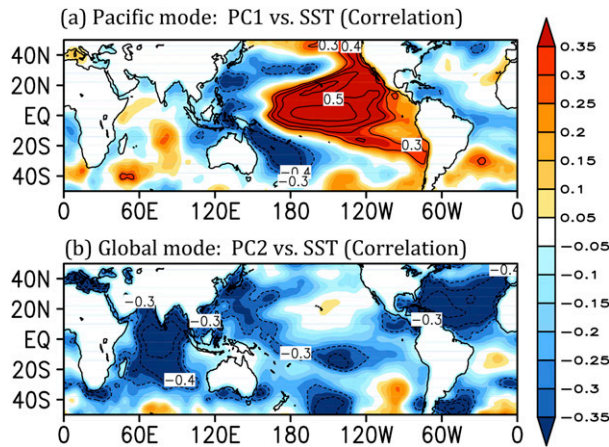(b) Global mode: PC2 vs. SST (Correlation)

FIG. 3. Correlation patterns of May–October average global SSTs with the principal component of (a) the first EOF mode (PC1) and (b) the second EOF mode (PC2) of May–October typhoon tracks over the western North Pacific. Correlation coefficients in contours are significant at the 95% confidence level.
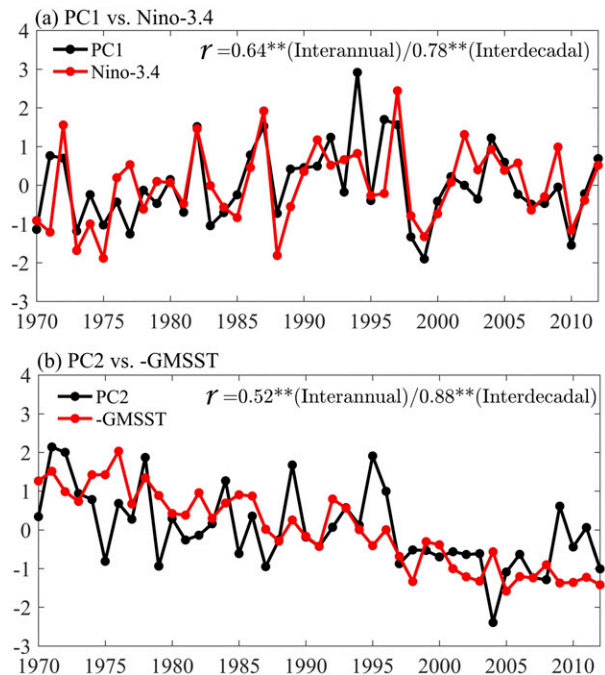
(a) PC1 vs. Nino-3.4

(b) PC2 vs. -GMSST

FIG. 4. (a) Time series of PC1 of May–October TC tracks over the western North Pacific and the May–October average Niño-3.4 index during 1970–2012. (b) As in (a), but for PC2 and the negative of May–October average global mean sea surface temperature ($-$GMSST). Correlation coefficients on the interannual and interdecadal time scales for the period of 1970–2012 are also displayed.

density as reported in Mei et al. (2015). This suggests a prevalence of the consistent basinwide pattern of TC track density anomalies over the WNP basin. A tripolar pattern for the second EOF mode resembles the second EOF modes in Liu and Chan (2008) which focuses on interdecadal variability, agreeing well with the significant interdecadal variability of the second EOF mode noted in this study (Fig. 3).

However, there are some differences between our study and these two studies. For example, the first EOF mode in this study is different from Liu and Chan (2008), although it does show some resemblance to both their first and third EOF modes. This could possibly be due to TC occurrence rates being normalized by annual TC counts prior to their EOF analyses. Additionally, our EOF-2nd also differs from that in Mei et al. (2015), which is likely associated with a focus on different time scales. Mei et al. (2015) performed an EOF analysis for both high-pass-filtered and low-pass-filtered fields, respectively, while our study directly conducted an EOF analysis based on observed TC occurrences. Moreover, different study periods and months being investigated may play a role in the differences from these previous studies.

These two EOF modes are largely determined by two distinct large-scale SSTA patterns (Fig. 3). As shown in Fig. 3a, the correlation pattern between the EOF-1st mode PC (hereafter PC1) and global SST is characterized by a tropical ENSO-like pattern (Wang and Chan 2002; Zhao and Wang 2019). There are significant positive correlations over the central-eastern tropical Pacific, and significant negative correlations in the western Pacific, especially in the subtropics. This ENSO-like pattern is present on both interannual and interdecadal time scales. There is a significant correlation between PC1 and the Niño-3.4 index (interannual correlation of 0.64 and an interdecadal correlation of 0.78) from 1970–2012 (Fig. 4a). Additionally, there is a significant correlation between PC1 and the PDO index on both interannual ($r = 0.33$) and

interdecadal ($r = 0.58$) time scales. Overall, the spatially consistent distribution of TC track patterns over the WNP basin as displayed by the EOF-1st mode is primarily determined by interannual and interdecadal changes in ENSO-like SSTA patterns.

The correlation pattern between PC2 and global SST during 1970–2012 is shown in Fig. 3b. These correlations show a same-signed pattern across most of the globe, with a significant correlation between PC2 and near-global mean SST over the oceanic domain between 40°S and 60°N (GMSST), both on interannual ($r = -0.52$) and interdecadal ($r = -0.88$) time scales (Fig. 4b). This consistent global pattern is also indicative of the long-term trend in GMSST (Fig. 4b). In summary, a nearly globally uniform SSTA pattern is closely related to a tripolar TC track change in the WNP, as highlighted by our EOF-2nd mode. Thus, we hypothesize that long-term warming caused by climate change may cause continued future tripolar TC track shifts.

We further conducted EOF analyses on TC occurrence during May–July and August–October, respectively and found that the first two leading EOF patterns were similar, both with respect to changes in their respective variances and the amplitudes of their EOF modes (Fig. S3). The EOF-1st mode during May–July is similar to EOF-2nd mode during the full season from May–October, with a tripolar pattern characterized by an increase in TC occurrences following track I, a weak
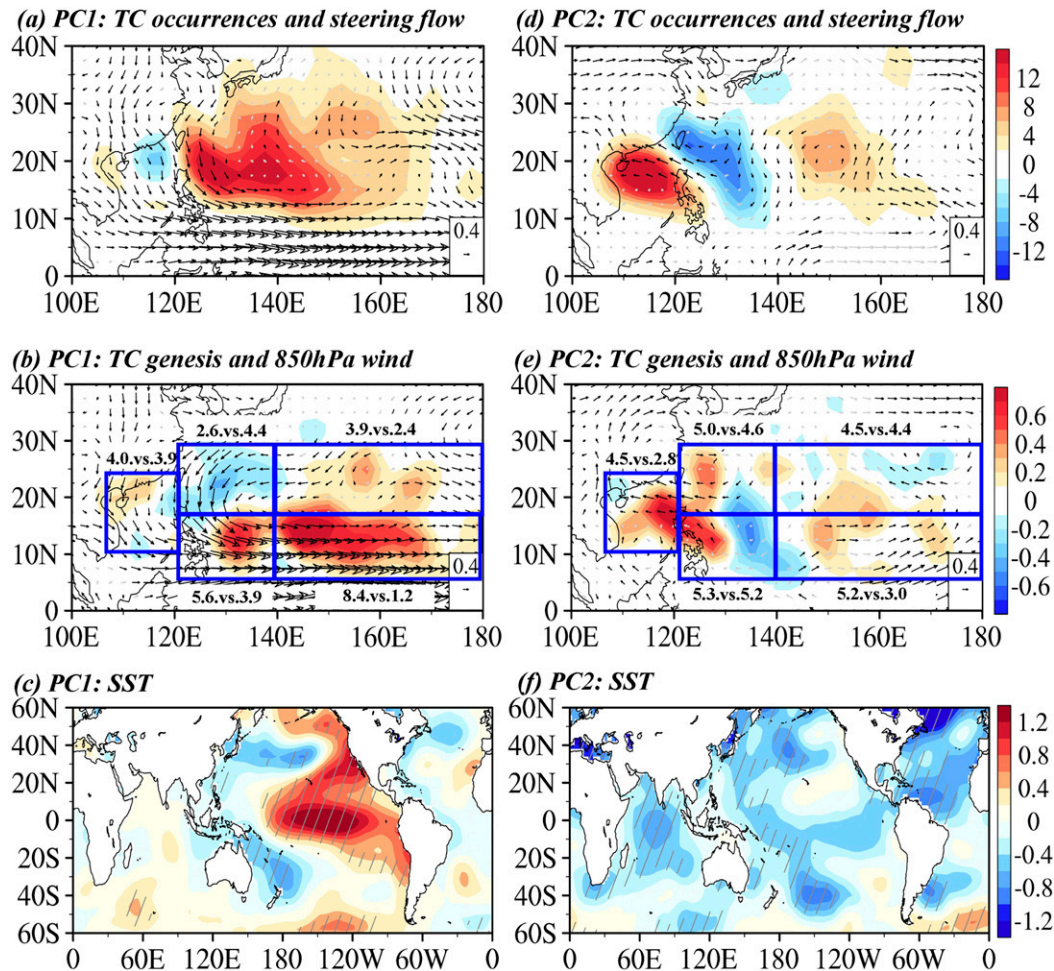
FIG. 5. Spatial difference of (a),(d) TC occurrences, (b),(e) TC counts, and (c),(f) SSTAs between years with positive and negative (left) PC1 and (right) PC2. Seven years with positive PC1 (i.e.,1982, 1987, 1992, 1994, 1996, 1997, and 2004) and eight years with negative PC1 (i.e.,1970, 1973, 1975, 1977, 1983, 1998, 1999, and 2010) are selected. Six years with positive PC2 (i.e.,1971, 1972, 1978, 1984, 1989, and 1995) and five years with negative PC2 (i.e.,2004, 2005, 2007, 2008, and 2012) are selected. The wind vectors in black and SSTAs with white diagonal hatching are significant at the 95% confidence level. The frequency of TC occurrence in this study, calculated as the accumulated TC track frequency, indicates how many TCs enter a specific grid box of 2.5° latitude × 2.5° longitude. The TC genesis location is defined as the point that each TC first reached named storm strength ($\geq 17.2\,\mathrm{m\,s^{-1}}$).

increase in TC occurrences following track III and a weak decrease in TC occurrences following track II (Fig. 1c and Fig. S3a). The EOF-2nd mode during May–July is similar to the EOF-1st mode for the full season from May to October. This pattern is dipole in nature and is characterized by a decrease in TC occurrences following TC track I and an increase in TC occurrences following TC tracks II and III (Fig. 1b and Fig. S3b). By contrast, the first two leading EOF modes during August–October are largely similar to the full season from May to October (Figs. S3c,d; Figs. 1b,c). The SST patterns associated with the principal components of the first two leading modes for May–July and August–October are also further examined. The PC2–SSTA correlation pattern during May–July is largely similar to the PC1–SSTA correlation pattern during August–October with respect to its amplitude (Figs. S4b,c). These

patterns show SSTAs typically associated with ENSO. Although the PC1–SSTA pattern during May–July and the PC2–SSTA pattern during August–October have some differences, they appear to be mostly consistent (Figs. S4a,d). Meanwhile, although many similarities between TC changes and their associated global SST patterns are found during these two seasons, there are also some differences present. Additional investigation on possible physical explanations for TC track changes over different seasons are warranted.

Composite and correlation analyses are further conducted to understand the ENSO-like (associated with EOF-1st mode) and global SST patterns (associated with EOF-2nd mode) responsible for changes in TC tracks over the WNP basin. As shown in Figs. 5a and 5b, composite differences between years with positive and negative PC1 show a small decrease in TC

occurrences over the SCS. This appears mainly to be associated with a decrease of TCs moving into the SCS from the rest of the WNP basin together with a cyclonic steering flow anomaly over the SCS. In this study, the large-scale steering flow is computed as the mean May–October flow averaged from 850 and 300 hPa. These steering flow levels have been used in several previous studies (Wu and Wang 2004; Wu et al. 2005; Zhao et al. 2010; Zhao and Wu 2014). We find no significant difference in TC counts over the SCS. Meanwhile, there is a basinwide increase in TC occurrences over the WNP basin following prevailing track II and track III TCs, which is largely explained by a significant increase in TCs over most of the WNP basin. The increase in TCs is especially pronounced over the southern part of the WNP. There is also an apparent cyclonic circulation anomaly over eastern Asia.

There is an increase in TC counts over the southeastern part of the WNP as well as over the SCS for years with positive PC2 relative to years with negative PC2, while there is a substantial decrease in TC genesis frequency over the region bounded by 5°–22.5°N, 130°–140°E. The steering flow anomaly during positive PC2 years compared to that during negative PC2 years shows a clear tripolar pattern, with a cyclonic circulation anomaly over the SCS and southeastern WNP basin and an anticyclonic circulation anomaly over East Asia (Fig. 5d). Correspondingly, there is a similar tripolar low-level circulation anomaly (Fig. 5e) and a tripolar pattern in TC genesis frequency anomalies over the tropical WNP basin. TC counts increase over the eastern WNP basin (5°–20°N, 145°–175°E) and around the SCS (10°–25°N, 105°–130°E) and decrease over the region bounded by 5°–20°N, 130°–140°E (Fig. 5e). Consequently, there is an increase in TC occurrences following track I and track III and a decrease in TC occurrences following track II over the WNP basin. Differences in the large-scale steering flow associated with the first two EOF modes are further confirmed by the correlation map between the corresponding principal components and the large-scale steering flow over the WNP basin (Fig. 6).

Consistent with the correlation map between PC1 or PC2 and global SST (Fig. 3), composite differences of global SSTAs between years with positive and negative PC1 (PC2) also show an ENSO-like (global SST) pattern (Figs. 5c,f). As suggested by previous studies (Wu and Wang 2004; Wang and Chan 2002; Zhao et al. 2010), there is a nearly basinwide increase in TC occurrences over the WNP basin and a significant increase in TC counts over the southeastern region of the WNP basin during El Niño years. El Niño years also typically have a cyclonic circulation anomaly over east Asia. Meanwhile, prior studies have documented that ENSO has no apparent impact on the total number of TCs over the WNP basin but significantly modulates TC formation location as well as the large-scale circulation (Lander 1994; Wang and Chan 2002; Wu and Wang 2004; Camargo and Sobel 2005; Zhao et al. 2010). Our results show consistency with changes in TC tracks and TC formation locations in response to an ENSO-like pattern.

As noted above, changes in the large-scale steering flow associated with the first two leading EOF modes play an important role in changing prevailing TC tracks. The steering flows at 850 (low level), 500 (midlevel), and 300 hPa (upper
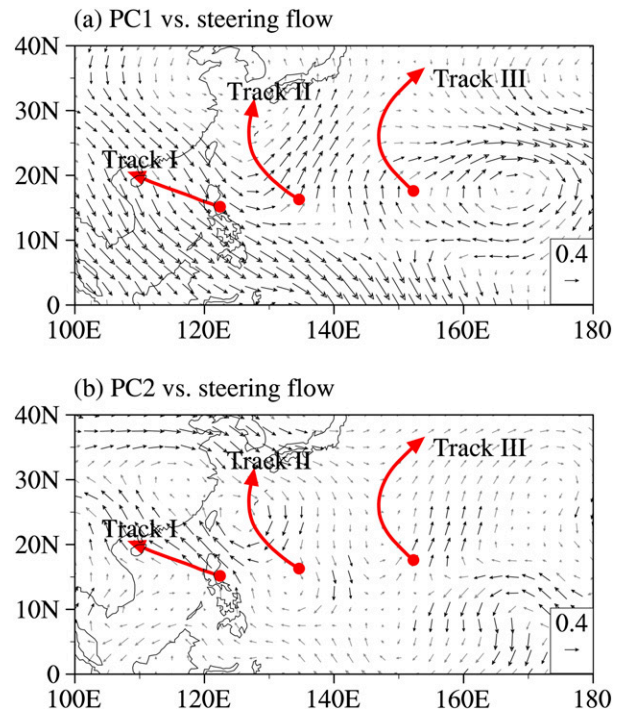

FIG. 6. Correlation pattern between (a) PC1 or (b) PC2 and the extended boreal summer (May–October) large-scale steering flow (vertically averaged from 850 to 300 hPa). Red lines indicate the three climatological prevailing TC tracks. The wind vectors in black represent correlations that are significant at the 95% confidence level.

level) are further examined to investigated possible changes in the large-scale circulation associated with the large-scale steering flow in response to the first two EOF modes. ENSO-like SSTA anomalies appear to induce changes in the WNP subtropical high and the South Asian high as well as low-level westerlies in the tropical WNP. These changes likely alter prevailing TC tracks (Figs. 7a,c,e). Decreased TC occurrences following TC track I are related to enhanced tropical westerlies at low levels induced by the increase in the SST gradient between the tropical western and central-eastern Pacific (Figs. 3a and 7a). The increase in TC occurrences following TC track II is mainly associated with an enhanced South Asian high induced by low-level Ekman pumping, which can also be seen from weak low to midlevel meridional wind and upper-level southerly wind anomalies around 140°E (Figs. 7a,c,e). The importance of the South Asian high can be inferred by the consistency between the upper-level horizontal wind and the large-scale steering flow (Figs. 6a and 7c). The enhanced subtropical high appears to be an important factor driving the increase of TC occurrences following TC track III, which is reflected in a better consistency between changes in the large-scale steering flow and 500-hPa zonal wind over the eastern WNP associated with PC1 (Figs. 6a and 7c). Opposite-signed circulation anomalies produced by Ekman pumping associated with enhanced low-level convergence induced by the tropical Pacific SST gradient also appear in the eastern WNP (east of
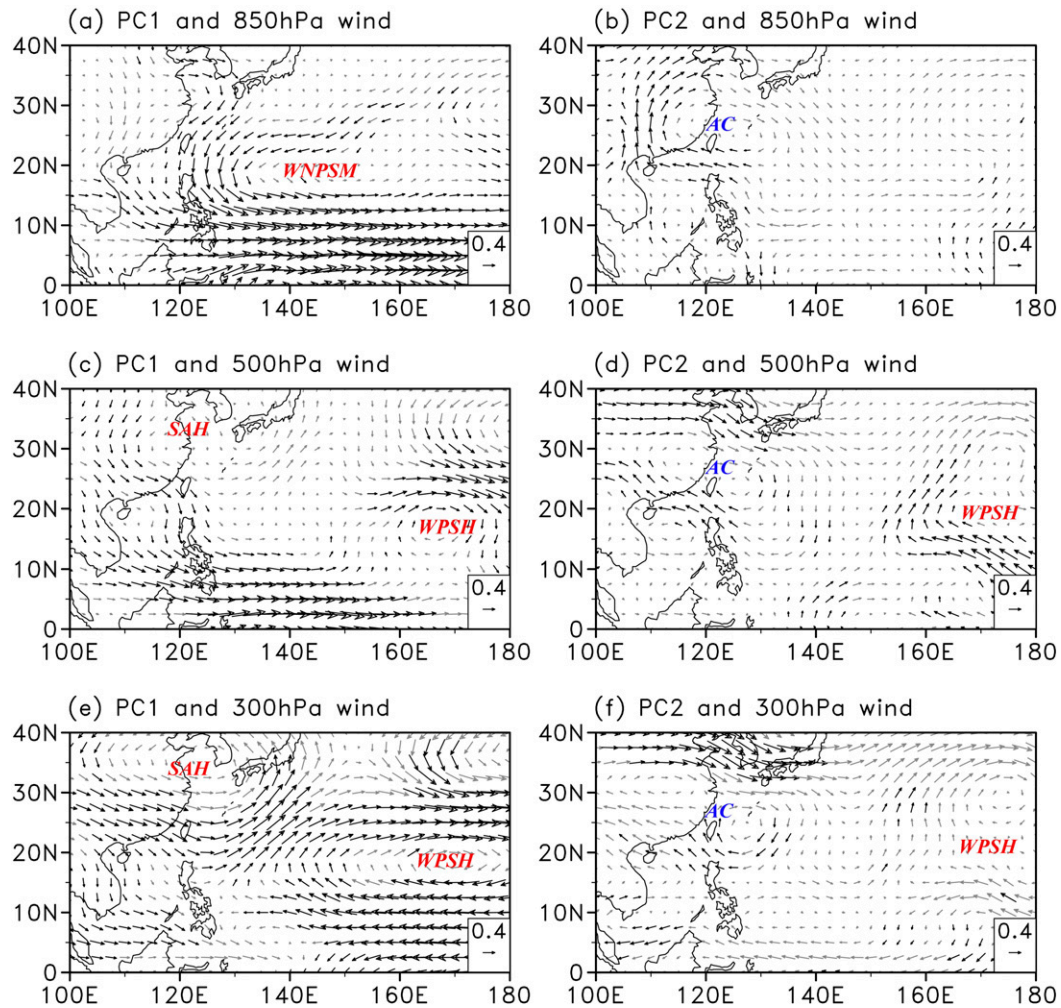
FIG. 7. Regression patterns of the extended boreal summer (May–October) averaged horizontal wind at (a),(b) 850, (c),(d) 500, and (e),(f) 300 hPa onto (left) PC1 and (right) PC2. The wind vectors in black represent significance at the 95% confidence level. AC indicates anticyclonic circulation anomalies, associated with PC2. WNPSM, WPSH, and SAH indicate the cyclonic circulation anomalies, anticyclonic circulations anomalies, and cyclonic circulation anomalies associated with each PC corresponding to the WNP summer monsoon, WNP subtropical high, and South Asian high, respectively.

145°E), with an associated low-level cyclonic and upper-level anticyclonic circulation (Figs. 7a,e), thus counteracting its contribution to the large-scale steering flow.

Changes in prevailing TC tracks associated with the second leading EOF mode are closely linked to the global SSTA pattern. The barotropic anticyclonic circulation over the western WNP basin is related to the observed land–sea thermal difference between East Asia and the western WNP basin. This leads to a weakened westward steering flow and increased TC occurrence following TC track I (Figs. 3b and 7b,d,f). The southward large-scale steering flow favors decreased TC occurrences following TC track II, which appears partly related to the climatological north–south SST gradient (Figs. 3b, 6b, and 7b,d,f). This southward flow has also been suggested in previous studies to be closely associated with global warming (Wang et al. 2012; Wu et al. 2005). When global SSTAs become consistently cooler, the north–south SST gradient in the western Pacific becomes stronger (Fig. 3b), thus enhancing

southward large-scale steering flow. Last, changes in track III are possibly associated with an enhancement of southwesterly large-scale steering flow (e.g., an anticyclonic circulation that is especially prominent in the middle to upper levels) (Figs. 7d,f) that appears to be linked to the apparent tripolar SSTA pattern over the eastern WNP (Fig. 3b).

Changes in prevailing TC tracks are generally due to combined changes in TC genesis location and large-scale steering flow associated with ENSO-like and global SSTA patterns. The next section therefore focuses on understanding the influence of ENSO-like and global SSTA patterns on interdecadal changes in extended boreal summer prevailing TC tracks over the WNP basin.

4. Observed interdecadal changes in TC tracks: Changing impact of ENSO-like and global SSTA patterns

Based upon the above analyses, the leading two EOF modes of WNP TC track change pattern are primarily controlled by
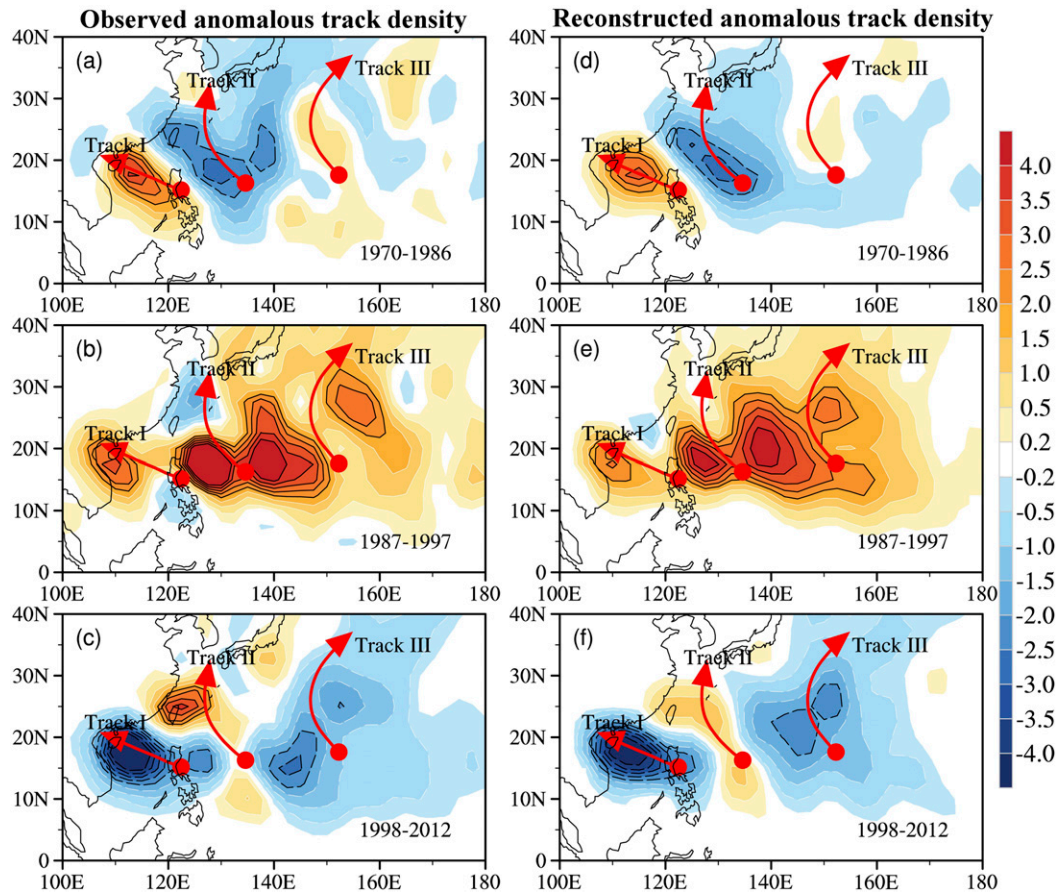
FIG. 8. Observed anomaly of May–October TC track density for the three epochs (a) 1970–86, (b) 1987–97, and (c) 1998–2012. (d)–(f) The corresponding reconstructed anomalies of May–October TC track density, which are only based on the first two leading EOF modes. The reconstructed expressions that are obtained by the least squares method for the three epochs are explicitly stated in the main text. The three prevailing typhoon tracks in red are displayed for reference, which are determined based on the climatological track density during 1970–2012. Contours indicate a significant value at the 95% confidence level from the observed and reconstructed climatology.

ENSO-like and consistent global SSTA patterns. As shown in Figs. 1e–h, the three distinct interdecadal epochs (1970–86, 1987–97, and 1998–2012) for WNP TC tracks can be easily identified from the evolution of these two EOF modes. In this section, our focus is to examine the ENSO-like and consistent global SSTA patterns and how they have affected the observed interdecadal change of WNP TC tracks with an emphasis on their respective importance. This can be deduced from the reconstructed track density anomalies based on the first two EOF modes for the different interdecadal epochs. The weights of the reconstruction expressions are determined using least squares fitting of the first two leading EOF modes onto the field of track density anomalies over the WNP basin for each of the three subperiods. As shown in Fig. 8, the reconstructed TC track density anomaly compares well with the observations for the three periods, raising our confidence in assessing the relative importance of the two large-scale SSTA modes (ENSO-like and consistent global) on the observed changes of WNP TC tracks.

During 1970–86, the observed track density anomaly shows a tripole pattern over the WNP basin (Fig. 8a). There is a

substantial increase in TC occurrences from the Philippine Sea to the SCS (track I) and a moderate increase of TCs with a prevailing recurving track (track III), while there is a decrease in TCs with a prevailing northwestward track (track II). During 1998–2012, the spatial distribution of observed TC track density anomalies appears to be the near opposite of the track change anomaly pattern during 1970–86 except for of a larger amplitude (Fig. 8c) in terms of the areas with significant differences. There is also good consistency as it relates to the large-scale steering flow, with anomalies of similar magnitude but of the opposite sign between 1970–86 and 1998–2012 (figure not shown). A tripole pattern in WNP TC tracks for these two periods suggests the dominance of the EOF-2nd mode. This was further confirmed by the reconstructed expressions $(0.35 \times \text{EOF-1st mode}) + (0.65 \times \text{EOF-2nd mode})$ for the period of 1970–86 (Fig. 8d) and $(-0.30 \times \text{EOF-1st mode}) - (0.70 \times \text{EOF-2nd mode})$ for the period of 1998–2012 (Fig. 8f). Correspondingly, the globe was characterized by relatively cool and warm SSTAs during 1970–86 (Fig. 9a) and 1998–2012 (Fig. 9c), respectively. Meanwhile, there is a cool maximum of
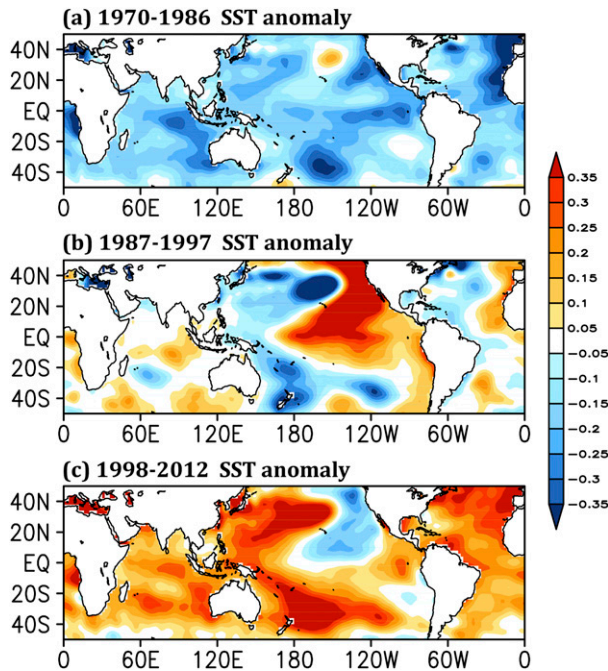
FIG. 9. May–October average global sea surface temperature anomaly (unit: °C) for (a) 1970–86, (b) 1987–97, and (c) 1998–2012 from the 1970–2012 climatological mean.

SSTA over the tropical equatorial central-eastern Pacific during 1970–86. The tropical central Pacific exhibits a relatively large cool SSTA pattern during 1998–2012 in agreement with previous studies on the cool PDO phase (Liu and Chan 2008; Zhao and Wang 2016, 2019) and an increasing occurrence of La Niña and central Pacific El Niño events during 1998–2012 (Ashok et al. 2007; Yu and Kao 2007; Kug et al. 2009; Lee and McPhaden 2010; Hu et al. 2018; Zhao and Wang 2019). In summary, the observed TC track changes during 1970–86 and 1998–2012 are primarily controlled by consistent cool and warm global SSTA patterns, respectively. The 1998–2012 period was also partly contributed to by an increase in the frequency of La Niña and central Pacific El Niño events.

In contrast, the observed TC track density anomaly over the WNP basin during 1987–97 shows a consistent increase of TC occurrences over the whole basin except a small decrease in the northern SCS and in the vicinity of Taiwan (Fig. 8b). This pattern is similar to the EOF-1st mode. The greater importance of the EOF-1st mode in changing WNP TC track during this period is also seen from the reconstructed expression $(0.64 \times \text{EOF-1st mode}) + (0.36 \times \text{EOF-2nd mode})$ (Fig. 8e). As expected, the SSTA pattern during 1987–97 shows a typical tropical El Niño–like pattern (Fig. 9b). These analyses suggest that the ENSO-like SSTA pattern became an important player in changing TC track patterns over the WNP basin during 1987–97, while the global SSTA pattern played a lesser role.

5. Summary and conclusions

This study attempts to explore the possible driving physical mechanisms of observed May–October TC track changes on interdecadal time scales over the WNP basin. Using

conventional EOF analyses, we find two primary modes of variability in summertime WNP TC tracks. The EOF-1st mode is characterized by a consistent spatial distribution of TCs across the WNP basin, while the EOF-2nd mode shows a tripole pattern. The correlation analyses that we conducted further indicate that the two EOF modes are dominated by two distinct large-scale SSTA patterns. The EOF-1st mode is mainly controlled by a tropical ENSO-like pattern that is primarily present on interdecadal time scales, in addition to its well-known role in interannual variability. In contrast, a consistent global SSTA pattern plays a dominant role in modulating the EOF-2nd mode. In addition to interannual and interdecadal time scales, the global SSTA variability relationship to the EOF-2nd mode for WNP TC is likely important for the impacts of climate change on future WNP TC tracks.

Based upon the evolution of these two EOF modes, changes in TC track patterns are separated into three distinct decadal epochs (1970–86, 1987–97, and 1998–2012). These three interdecadal periods are consistent with previous studies (Chan 2008; Liu and Chan 2008; Zhao and Wang 2016, 2019). In terms of both the observed and the reconstructed TC track density anomalies for the three periods, the changing impacts of ENSO-like and consistent global SSTA patterns on interdecadal changes of WNP TC tracks are further assessed. The interdecadal changes of TC tracks are largely modulated by changes in the relative contribution of ENSO-like and consistent global SSTA patterns. A consistent cool SSTA over the globe played a larger role than the prevailing La Niña–like pattern in changing WNP TC tracks during 1970–86. During 1998–2012, a consistent warm global SSTA pattern showed a dominant impact in modulating TC track changes with a relatively small impact from the La Niña–like pattern that predominated during 1998–2012. In contrast, TC track changes during 1987–97 were mainly attributed to changes in the tropical ENSO-like pattern, with El Niño conditions tending to dominate during this epoch. Associated with an increase in global SST, we hypothesize that the trend in TC track density anomaly has a tripole pattern similar to the EOF-2nd mode. As expected, a tripole pattern is present for the trend in TC track density anomalies over the WNP basin in response to the global trend of SST warming (Fig. 10). Specifically, the prevailing westward and recurving TC tracks tend to increase (decrease) and the prevailing northward TC tracks tends to decrease (increase), comparing well with previous studies on northward and recurving TC tracks (tracks II and track III) tending to shift westward, whereas prevailing westward TCs (track I) tend to shift northward (Wu et al. 2005; Zhao and Wu 2014; Wang et al. 2011). Additionally, when global SSTs are cooler, there is also statistically significant decreased SST found in specific regions such as the tropical Indian Ocean, the equatorial central Pacific, the WNP, and the North Atlantic (Figs. 3b and 5f). The relative importance of changes in these other regions and their impacts on WNP TC track warrant further investigation.

There is a significant correlation ($r = -0.88$) between PC2 and GMSST on an interdecadal time scale (9-yr running average) (Fig. 4b), while there is a clear increasing (decreasing) trend in GMSST (PC2). We further removed their linear trends
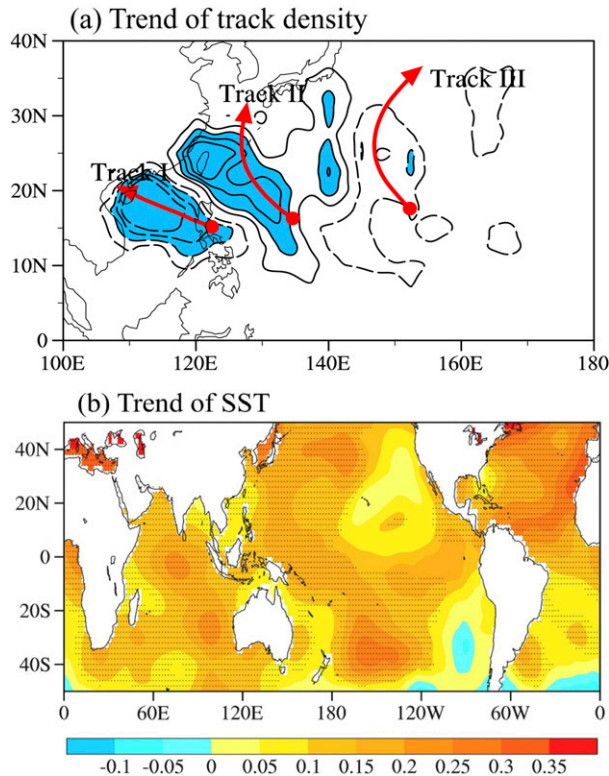
FIG. 10. (a) Trend of May–October typhoon track density over the western North Pacific (contours; unit: yr^{-1}) and (b) the trend in global sea surface temperature (unit: $°\text{C decade}^{-1}$) during 1970–2012. Shading in (a) and stippling in (b) indicate a significant trend in May–October track density and SST at the 95% confidence level, respectively.

and also found a significant correlation (-0.53) between the two indices (Fig. 11). The absolute value of the correlation between the two indices with the linear trend removed is substantially smaller than the absolute value of the correlation without removal of the linear trend. We also find that the amplitude of the SSTAs with removal of the linear trend is smaller compared to the SSTA amplitude without removal of
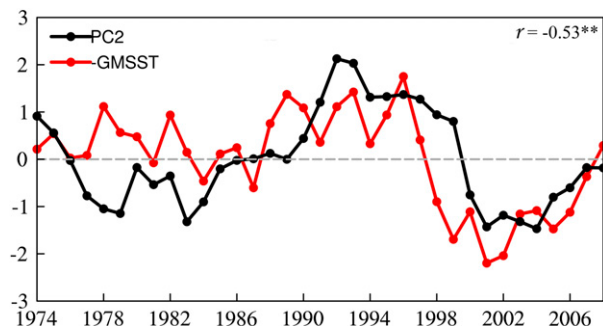

FIG. 11. Normalized time series of detrended 9-yr running-average PC2 and minus GMSST ($-$GMSST) during 1970–2012. The correlation between PC2 and GMSST is -0.53, which is significant at the 95% confidence level.
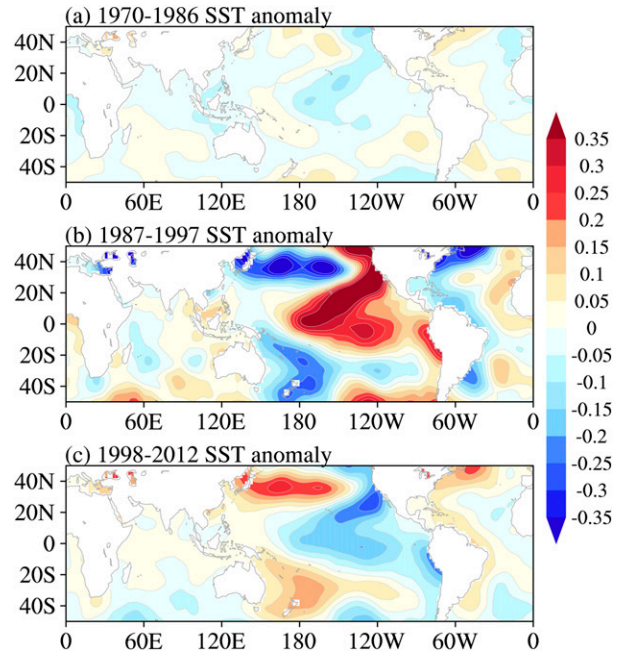

FIG. 12. Detrended May–October averaged SSTA (unit: °C) for (a) 1970–86, (b) 1987–97, and (c) 1998–2012, respectively, from the climatological mean of 1970–2012.

the linear trend. Moreover, the SSTA pattern without the linear trend exhibits a clearer cool PDO-like pattern during 1970–86 and 1998–2012 and a clearer warm PDO-like pattern during 1987–97 (Fig. 12). We hypothesize from this analysis that global warming may change the effect of global SSTA and ENSO-like patterns on future changes in prevailing TC tracks over the WNP basin.

Additionally, we calculated the 11-yr running average amplitude of the multivariate ENSO index (Wolter and Timlin 1998) during 1970–2012 and found a peak ENSO amplitude during 1987–97 (Fig. S5), which is consistent with the dominance of TC tracks associated with the ENSO-like SSTA pattern. We then correlated the 9-point running mean of PCs with the trend included and the trend removed for the first two leading modes in this study with global SSTA. PC1 and PC2 with the trend removed demonstrate an SSTA correlation pattern similar to the decadal ENSO mode (Figs. S6c,d), while the PC1/PC2 with the trend included-SSTA correlation pattern displays a globally consistent mode (Figs. S6a,b). To further confirm these findings, an EOF analysis for the 9-yr running mean of TC occurrences with the trend included and the trend removed during 1970–2012 is directly performed, and similar results can be found (Fig. S7). On the interannual time scale, an ENSO-like pattern between PC1/PC2 and global SSTA (Fig. S8) is observed. In terms of the pattern consistency between PCs and SSTA correlation maps on various time scales from interannual to decadal (Figs. S6, S7, and S8) and the raw correlation shown in Fig. 3 of this study, we infer that TC tracks associated with the EOF-1st mode are mainly associated with the ENSO mode on interdecadal and interannual time scales,

while the TC tracks associated with the EOF-2nd mode are mainly associated with a globally consistent mode. Note that these analyses are causal and are statistical in nature. More observational analyses and numerical simulations are needed to confirm these results.

In summary, these results suggest that WNP TC track changes on various time scales are dominated by the prevalence of ENSO-like and consistent global SSTA patterns. The findings of this study shed light on WNP TC track changes in response to climate change that would be helpful for climate prediction and for future projections of TC tracks over the WNP basin. Consequently, these findings are of potentially significant socioeconomic merit. We also caution that TC activity may pose a possible increased threat to East Asia under continued global warming. The possible impact of different seasons on the results of this study as well as to how different time scales (e.g., interannual, interdecadal, long-term trend) contribute to TC track changes deserve further investigation.

REFERENCES

Anderson, J. R., and J. R. Gyakum, 1989: A diagnostic study of Pacific basin circulation regimes as determined from extratropical cyclone tracks. *Mon. Wea. Rev.*, **117**, 2672–2686, https://doi.org/10.1175/1520-0493(1989)117<2672:ADSOPB>2.0.CO;2.

Ashok, K., S. K. Behera, S. A. Rao, H. Weng, and T. Yamagata, 2007: El Niño Modoki and its possible teleconnection. *J. Geophys. Res.*, **112**, C11007, https://doi.org/10.1029/2006JC003798.

Camargo, S. J., and A. H. Sobel, 2005: Western North Pacific tropical cyclone intensity and ENSO. *J. Climate*, **18**, 2996–3006, https://doi.org/10.1175/JCLI3457.1.

——, A. W. Robertson, S. J. Gaffney, P. Smyth, and M. Ghil, 2007a: Cluster analysis of typhoon tracks. Part I: General properties. *J. Climate*, **20**, 3635–3653, https://doi.org/10.1175/JCLI4188.1.

——, ——, ——, ——, and ——, 2007b: Cluster analysis of typhoon tracks. Part II: Large-scale circulation and ENSO. *J. Climate*, **20**, 3654–3676, https://doi.org/10.1175/JCLI4203.1.

——, A. H. Sobel, A. D. Delgenio, J. A. Jonas, M. Kelley, Y. Lu, D. A. Shaevitz, and N. Henderson, 2016: Tropical cyclones in the GISS ModelE2. *Tellus*, **68A**, 31494, https://doi.org/10.3402/tellusa.v68.31494.

Chan, J. C. L., 2008: Decadal variations of intense typhoon occurrence in the western North Pacific. *Proc. Roy. Soc.*, **464A**, 249–272, https://doi.org/10.1098/rspa.2007.0183.

Chen, T. C., S. Y. Wang, M. C. Yen, and A. J. Clark, 2009: Impact of the intraseasonal variability of the western North Pacific large-scale circulation on tropical cyclone tracks. *Wea. Forecasting*, **24**, 646–666, https://doi.org/10.1175/2008WAF2222186.1.

Chu, J.-H., C. R. Sampson, A. S. Levine, and E. Fukada, 2002: The Joint Typhoon Warning Center tropical cyclone best-tracks, 1945–2000. Naval Research Laboratory Rep. NRL/MR/7540-02-16, 22 pp.

Elsner, J. B., 2003: Tracking hurricanes. *Bull. Amer. Meteor. Soc.*, **84**, 353–356, https://doi.org/10.1175/BAMS-84-3-353.

——, and K.-B. Liu, 2003: Examining the ENSO–typhoon hypothesis. *Climate Res.*, **25**, 43–54, https://doi.org/10.3354/cr025043.

Emanuel, K. A., 2005: Increasing destructiveness of tropical cyclones over the past 30 years. *Nature*, **436**, 686–688, https://doi.org/10.1038/nature03906.

Fudeyasu, H., S. Iizuka, and T. Matsuura, 2006: Impact of ENSO on landfall characteristics of tropical cyclones over the western North Pacific during the summer monsoon season. *Geophys. Res. Lett.*, **33**, L21815, https://doi.org/10.1029/2006GL027449.

Ha, Y., Z. Zhong, Y. Hu, and X. Yang, 2013: Influences of ENSO on western North Pacific tropical cyclone kinetic energy and its meridional transport. *J. Climate*, **26**, 322–332, https://doi.org/10.1175/JCLI-D-11-00543.1.

Ho, C.-H., J.-J. Baik, J.-H. Kim, D.-Y. Gong, and C.-H. Sui, 2004: Interdecadal changes in summertime typhoon tracks. *J. Climate*, **17**, 1767–1776, https://doi.org/10.1175/1520-0442(2004)017<1767:ICISTT>2.0.CO;2.

Hu, C., C. Zhang, S. Yang, D. Chen, and S. He, 2018: Perspective on the northwestward shift of autumn tropical cyclogenesis locations over the western North Pacific from shifting ENSO. *Climate Dyn.*, **51**, 2455–2465, https://doi.org/10.1007/s00382-017-4022-1.

Huang, B., and Coauthors, 2015: Extended Reconstructed Sea Surface Temperature version 4 (ERSST.v4). Part I: Upgrades and intercomparisons. *J. Climate*, **28**, 911–930, https://doi.org/10.1175/JCLI-D-14-00006.1.

IPCC, 2013: *Climate Change 2013: The Physical Science Basis*. T. F. Stocker et al., Eds., Cambridge University Press, 1535 pp.

Kanamitsu, M., W. Ebisuzaki, J. Woollen, S.-K. Yang, J. J. Hnilo, M. Fiorino, and G. L. Potter, 2002: NCEP–DOE AMIP-II Reanalysis (R-2). *Bull. Amer. Meteor. Soc.*, **83**, 1631–1644, https://doi.org/10.1175/BAMS-83-11-1631.

Kim, H.-K., and K.-H. Seo, 2016: Cluster analysis of tropical cyclone tracks over the western North Pacific using a self-organizing map. *J. Climate*, **29**, 3731–3751, https://doi.org/10.1175/JCLI-D-15-0380.1.

Kim, H.-S., J.-H. Kim, C.-H. Ho, and P.-S. Chu, 2011: Pattern classification of typhoon tracks using the fuzzy *c*-means clustering method. *J. Climate*, **24**, 488–508, https://doi.org/10.1175/2010JCLI3751.1.

Kim, J.-H., C.-H. Ho, and P.-S. Chu, 2010: Dipolar redistribution of summertime tropical cyclone genesis between the Philippine Sea and the northern South China Sea and its possible mechanisms. *J. Geophys. Res.*, **115**, D06104, https://doi.org/10.1029/2009JD012196.

Knutson, T. R., and R. E. Tuleya, 2004: Impact of CO_2-induced warming on simulated hurricane intensity and precipitation: Sensitivity to the choice of climate model and convective parameterization. *J. Climate*, **17**, 3477–3495, https://doi.org/10.1175/1520-0442(2004)017<3477:IOCWOS>2.0.CO;2.

——, and Coauthors, 2010: Tropical cyclones and climate change. *Nat. Geosci.*, **3**, 157–163, https://doi.org/10.1038/ngeo779.

——, and Coauthors, 2019: Tropical cyclones and climate change assessment: Part I. Detection and attribution. *Bull. Amer. Meteor. Soc.*, **100**, 1987–2007, https://doi.org/10.1175/BAMS-D-18-0189.1.

——, and Coauthors, 2020: Tropical cyclones and climate change assessment: Part II. Projected response to anthropogenic warming. *Bull. Amer. Meteor. Soc.*, **101**, E303–E322, https://doi.org/10.1175/BAMS-D-18-0194.1.

Kug, J.-S., K. P. Sooraj, D. Kim, I.-S. Kang, F.-F. Jin, Y. N. Takayabu, and M. Kimoto, 2009: Simulation of state dependent high-frequency atmospheric variability associated with ENSO. *Climate Dyn.*, **32**, 635–648, https://doi.org/10.1007/s00382-008-0434-2.

Lander, M. A., 1994: Description of a monsoon gyre and its effects on the tropical cyclones in the western North Pacific during August 1991. *Wea. Forecasting*, **9**, 640–654, https://doi.org/10.1175/1520-0434(1994)009<0640:DOAMGA>2.0.CO;2.

Lee, T., and P. Cornillon, 1995: Temporal variation of meandering intensity and domain-wide lateral oscillations of the Gulf Stream. *J. Geophys. Res.*, **100**, 13 603–13 613, https://doi.org/10.1029/95JC01219.

——, and M. J. McPhaden, 2010: Increasing intensity of El Niño in the central-equatorial Pacific. *Geophys. Res. Lett.*, **37**, L14603, https://doi.org/10.1029/2010GL044007.

Li, R. C., and W. Zhou, 2013: Modulation of western North Pacific tropical cyclone activity by the ISO. Part II: Tracks and landfalls. *J. Climate*, **26**, 2919–2930, https://doi.org/10.1175/JCLI-D-12-00211.1.

Li, W., L. Li, and Y. Deng, 2015: Impact of the interdecadal Pacific oscillation on tropical cyclone activity in the North Atlantic and eastern North Pacific. *Sci. Rep.*, **5**, 12358, https://doi.org/10.1038/srep12358.

Liu, K. S., and J. C. Chan, 2008: Interdecadal variability of western North Pacific tropical cyclone tracks. *J. Climate*, **21**, 4464–4476, https://doi.org/10.1175/2008JCLI2207.1.

Liu, W., and Coauthors, 2015: Extended reconstructed sea surface temperature version 4 (ERSST.v4): Part II. Parametric and structural uncertainty estimations. *J. Climate*, **28**, 931–951, https://doi.org/10.1175/JCLI-D-14-00007.1.

Mantua, N. J., S. R. Hare, Y. Zhang, J. M. Wallace, and R. C. Francis, 1997: A Pacific interdecadal climate oscillation with impacts on salmon production. *Bull. Amer. Meteor. Soc.*, **78**, 1069–1080, https://doi.org/10.1175/1520-0477(1997)078<1069:APICOW>2.0.CO;2.

Mei, W., S.-P. Xie, M. Zhao, and Y. Wang, 2015: Forced and internal variability of tropical cyclone track density in the western North Pacific. *J. Climate*, **28**, 143–167, https://doi.org/10.1175/JCLI-D-14-00164.1.

Murakami, H., B. Wang, and A. Kitoh, 2011: Future change of western North Pacific typhoons: Projections by a 20-km-mesh global atmospheric model. *J. Climate*, **24**, 1154–1169, https://doi.org/10.1175/2010JCLI3723.1.

——, E. Levin, T. L. Delworth, R. Gudgel, and P.-C. Hsu, 2018: Dominant effect of relative tropical Atlantic warming on major hurricane occurrence. *Science*, **362**, 794–799, https://doi.org/10.1126/science.aat6711.

North, G. R., T. L. Bell, R. F. Cahalan, and F. J. Moeng, 1982: Sampling errors in the estimation of empirical orthogonal functions. *Mon. Wea. Rev.*, **110**, 699–706, https://doi.org/10.1175/1520-0493(1982)110<0699:SEITEO>2.0.CO;2.

Rasmusson, E. M., P. A. Arkin, W. Y. Chen, and J. B. Jalickee, 1981: Biennial variations in surface temperature over the United States as

revealed by singular decomposition. *Mon. Wea. Rev.*, **109**, 587–598, https://doi.org/10.1175/1520-0493(1981)109<0587:BVISTO>2.0.CO;2.

Saunders, M. A., R. E. Chandler, C. J. Merchant, and F. P. Roberts, 2000: Atlantic hurricanes and NW Pacific typhoons: ENSO spatial impacts on occurrence and landfall. *Geophys. Res. Lett.*, **27**, 1147–1150, https://doi.org/10.1029/1999GL010948.

Schreck, C. J., K. R. Knapp, and J. P. Kossin, 2014: The impact of best track discrepancies on global tropical cyclone climatologies using IBTrACS. *Mon. Wea. Rev.*, **142**, 3881–3899, https://doi.org/10.1175/MWR-D-14-00021.1.

Tu, J.-Y., C. Chou, and P.-S. Chu, 2009: The abrupt shift of typhoon activity in the vicinity of Taiwan and its association with western North Pacific–East Asian climate change. *J. Climate*, **22**, 3617–3628, https://doi.org/10.1175/2009JCLI2411.1.

Wang, B., and J. C. L. Chan, 2002: How strong ENSO events affect tropical storm activity over the western North Pacific. *J. Climate*, **15**, 1643–1658, https://doi.org/10.1175/1520-0442(2002)015<1643:HSEEAT>2.0.CO;2.

——, Z. Wu, J. Li, J. Liu, C. P. Chang, Y. Ding, and G. Wu, 2008: How to measure the strength of the East Asian summer monsoon. *J. Climate*, **21**, 4449–4463, https://doi.org/10.1175/2008JCLI2183.1.

——, J. Liu, H.-J. Kim, P. J. Webster, and S.-Y. Yim, 2012: Recent change of the global monsoon precipitation (1979–2008). *Climate Dyn.*, **39**, 1123–1135, https://doi.org/10.1007/s00382-011-1266-z.

Wang, C., and B. Wang, 2019: Tropical cyclone predictability shaped by western Pacific subtropical high: integration of trans-basin sea surface temperature effects. *Climate Dyn.*, **53**, 2697–2714, https://doi.org/10.1007/s00382-019-04651-1.

——, ——, and L. Wu, 2019: A region-dependent seasonal forecasting framework for tropical cyclone genesis frequency in the western North Pacific. *J. Climate*, **32**, 8415–8435, https://doi.org/10.1175/JCLI-D-19-0006.1.

Wang, R., L. Wu, and C. Wang, 2011: Typhoon track changes associated with global warming. *J. Climate*, **24**, 3748–3752, https://doi.org/10.1175/JCLI-D-11-00074.1.

Webster, P. J., G. J. Holland, J. A. Curry, and H. R. Chang, 2005: Changes in tropical cyclone number, duration, and intensity in a warming environment. *Science*, **309**, 1844–1846, https://doi.org/10.1126/science.1116448.

Wolter, K., and M. S. Timlin, 1998: Measuring the strength of ENSO events: How does 1997/98 rank? *Weather*, **53**, 315–324, https://doi.org/10.1002/j.1477-8696.1998.tb06408.x.

Wu, L., and B. Wang, 2004: Assessing impacts of global warming on tropical cyclone tracks. *J. Climate*, **17**, 1686–1698, https://doi.org/10.1175/1520-0442(2004)017<1686:AIOGWO>2.0.CO;2.

——, and ——, 2008: What has changed the proposition of intense hurricanes in the last 30 years? *J. Climate*, **21**, 1432–1439, https://doi.org/10.1175/2007JCLI1715.1.

——, and H. Zhao, 2012: Dynamically derived tropical cyclone intensity changes over the western North Pacific. *J. Climate*, **25**, 89–98, https://doi.org/10.1175/2011JCLI4139.1.

——, B. Wang, and S. Geng, 2005: Growing typhoon influence on East Asia. *Geophys. Res. Lett.*, **32**, L18703, https://doi.org/10.1029/2005GL022937.

——, ——, and S. A. Braun, 2008: Implications of tropical cyclone power dissipation index. *Int. J. Climatol.*, **28**, 727–731, https://doi.org/10.1002/joc.1573.

——, C. Wang, and B. Wang, 2015: Westward shift of western North Pacific tropical cyclogenesis. *Geophys. Res. Lett.*, **42**, 1537–1542, https://doi.org/10.1002/2015GL063450.

——, R. Wang, and X. Feng, 2018: Dominant role of the ocean mixed layer depth in the increased proportion of intense typhoons

during 1980–2015. *Earth's Future*, **6**, 1518–1527, https://doi.org/10.1029/2018EF000973.

Yu, J.-Y., and H.-Y. Kao, 2007: Decadal changes of ENSO persistence barrier in SST and ocean heat content indices: 1958–2001. *J. Geophys. Res.*, **112**, D13106, https://doi.org/10.1029/2006JD007654.

Zhan, R.-F., Y. Wang, and X.-T. Lei, 2011: Contributions of ENSO and East Indian Ocean SSTA to the interannual variability of northwest Pacific tropical cyclone frequency. *J. Climate*, **24**, 509–521, https://doi.org/10.1175/2010JCLI3808.1.

Zhang, J., L. Wu, and Q. Zhang, 2011: Tropical cyclone damages in China under the background of global warming. *J. Trop. Meteor.*, **27**, 442–454.

Zhang, Q., L. Wu, and Q. Liu, 2009: Tropical cyclone damages in China 1983–2006. *Bull. Amer. Meteor. Soc.*, **90**, 489–496, https://doi.org/10.1175/2008BAMS2631.1.

Zhao, H., 2016: A downscaling technique to simulate changes in western North Pacific tropical cyclone activity between two types of El Niño events. *Theor. Appl. Climatol.*, **123**, 487–501, https://doi.org/10.1007/s00704-015-1374-5.

——, and L. Wu, 2014: Inter-decadal shift of the prevailing tropical cyclone tracks over the western North Pacific and its mechanism study. *Meteor. Atmos. Phys.*, **125**, 89–101, https://doi.org/10.1007/s00703-014-0322-8.

——, and C. Wang, 2016: Interdecadal modulation on the relationship between ENSO and typhoon activity during the late season in the western North Pacific. *Climate Dyn.*, **47**, 315–328, https://doi.org/10.1007/s00382-015-2837-1.

——, and ——, 2019: On the relationship between ENSO and tropical cyclones in the western North Pacific during the boreal summer. *Climate Dyn.*, **52**, 275–288, https://doi.org/10.1007/s00382-018-4136-0.

——, L. Wu, and W. Zhou, 2009: Observational relationship of climatologic beta drift with large-scale environmental flows. *Geophys. Res. Lett.*, **36**, L18809, https://doi.org/10.1029/2009GL040126.

——, ——, and ——, 2010: Assessing the influence of the ENSO on tropical cyclone prevailing tracks in the western North Pacific. *Adv. Atmos. Sci.*, **27**, 1361–1371, https://doi.org/10.1007/s00376-010-9161-9.

——, ——, and ——, 2011: Interannual changes of tropical cyclone intensity in the western North Pacific. *J. Meteor. Soc. Japan*, **89**, 243–253, https://doi.org/10.2151/JMSJ.2011-305.

——, ——, and R. Wang, 2014: Decadal variations of intense tropical cyclones over the western North Pacific during 1948–2010. *Adv. Atmos. Sci.*, **31**, 57–65, https://doi.org/10.1007/s00376-013-3011-5.

——, X. Duan, G. B. Raga, and P. J. Klotzbach, 2018: Changes in characteristics of rapidly intensifying western North Pacific tropical cyclones related to climate regime shifts. *J. Climate*, **31**, 8163–8179, https://doi.org/10.1175/JCLI-D-18-0029.1.